Geotech Geol Eng (2020) 38:4617–4635
https://doi.org/10.1007/s10706-020-01314-5

ORIGINAL PAPER

# Analysing Rectangular Pile Using One Dimensional Finite Element

**M. El Gendy · H. Ibrahim · I. El Arabi**

Received: 23 October 2019 / Accepted: 13 April 2020 / Published online: 24 April 2020


**Abstract** The traditional methods for analysing rectangular piles (Barrettes) are mainly modelling the barrette and surrounding soil using 3D-FE. 3D-FE for barrette foundations needs a huge computational effort. Consequently, a huge system of equations required to be solved. In this paper, a composed coefficient technique (CCT) is developed for analysing laterally loaded barrettes. The technique takes into account the three-dimensional full interactions between the barrette and the surrounding soil. In the technique, the three dimensional coefficients of the stiffness matrix of the barrette are decomposed to be one-dimensional. This enables easily adding these coefficients to those of stiffness matrix of the soil. Besides the practical application and efficiency of the technique, the nonlinear response of the barrette using any load-settlement relation can be considered. The technique may be also applied for single barrette, barrette groups or barrette raft. A series of validations is carried out to verify the application of CCT for analysing single barrettes. It is found that treating the barrette by CCT, gives nearly the same results compared with the measured values from load tests and FE results. The proposed technique is implemented in the program ELPLA El Gendy M and El Gendy A (Analysis and design of raft and piled Raft-Program ELPLA, GEOTEC Software Inc., Calgary, 2019).

**Keywords** Soil structure interaction · Deep foundation · Rectangular pile · Barrette · Single barrette · Composed coefficient technique

## 1 Introduction

Early researches on single barrettes were performed using 3D-FE to analyse single barrette. This technique takes into account full interactions between barrettes and the surrounding soil, but it leads to a huge stiffness matrix. Therefore, huge systems of equations have to be solved. Consequently, this analysis is time consuming even for the fast computers of today. A similar foundation element of pile maybe considered as a less complicated problem than that of the barrette cross section. Piles, in most cases, are circular in shape with small cross-sectional area, while that of the barrette is mainly rectangular, with large cross-sectional area. Therefore, the pile can be treated as a beam member subjected to point loads on its nodes, while barrettes are treated as block members. Many methods are available for the analysis of piles, most of them are used also to analyse barrettes with equivalent cross section area to that of the pile.

M. El Gendy (✉) · H. Ibrahim · I. El Arabi
Department of Civil Engineering, Faculty of Engineering, Port Said University, Port Said, Egypt
e-mail: mahmoud.mohamed@eng.psu.edu.eg

Thasnanipan et al. (1998) reported construction practice and the performance of barrette constructed in Bangkok metropolis. Using trial trenching near a canal for assessment of trench stability and soil deformation. Also discussed choice of barrette and common defects found in barrette.

Zhang (2003) performed a 3D analysis of two laterally loaded barrettes tested in Hong Kong using FLPIER software based on p-y curves. He reported that the lateral response of the barrette is influenced by loading direction and the lateral load capacity is the greatest when the loading is along the major axis. Similar results were reported by El Wakil and Nazir (2013) on a small scale model of barrette tested in laboratory.

Lei et al. (2007) presented an approximate three-dimensional semi analytical method for the analysis of load–displacement behaviour of single barrettes, barrette group and barrette-soil-cap interaction system.

Basu et al. (2008, 2007, 2008), Choi et al. (2014, 2015) and Seo et al. (2009) developed an analysis for laterally and vertically loaded piles and barrettes embedded in a multi-layered soil medium, based on the solution of differential equations governing the displacements of the pile-soil system derived from energy principles.

Lin et al. (2014) studied the axial performance of two heavily instrumented barrettes, with and without grouting, socket into gravel layer in Taipei, which is evaluated based on the results of barrette load tests. And also simulated the t–z curves interpreted from the measured data along depth by the hyperbolic model.

Conte et al. (2013) proposed a 3D-FE approach to predict the response of reinforced concrete piles to horizontal loading. Then he used the proposed approach to analyse the results from some loading tests documented concerning a large-diameter pile and a large-section rectangular pile (barrette) embedded in sandy soils.

Rafa and Moussai (2018) use Plaxis 3D to evaluate the interaction between barrette load test and the reaction system using the finite element code by comparing load test results in Bangkok, Thailand subsoil with those using the Hardening Soil model (HS).

Znamenskii et al. (2019) use MIDAS GTS NX to show the principal possibility of application of this method for the analyses of barrettes with an accuracy admissible for practical purposes by comparing barrette load test results in Moscow, Russia subsoil with those using a modified Mohr–Coulomb elastoplastic.

Poulos and Small (2019) examined the use of simple means of analysis based on conventional piles of circular cross-section by chosen equivalent dimensions for the circular piles to represent the barrette. They compared the behaviour of the equivalent piles to finite element results for the barrettes.

Composed Coefficient Technique (*CCT*) developed by El Gendy (2007) was a modification of the technique proposed by Russo (1998). El Gendy (2007) applied the technique on single pile, pile group and piled raft to reduce the size of the entire soil stiffness matrix. In this technique, the pile is treated as a rigid member having uniform settlement for all nodes along its shaft and base. *CCT* enables to assemble pile coefficients in composed coefficients. This technique was examined and applied efficiently in many studies, some of them are those by Abdel et al. (2009), Rabiei (2015), Rabiei and Choobbasti (2018, 2019), El Kamash et al. (2014), Ibrahim et al. (2009), El Gendy et al. (2010a, b, 2013, 2014), Mohamedien et al. (2013).

Recently, this technique is also further developed by El Gendy et al. (2016, 2017, 2018, 2019) to be used for analysing single barrettes under vertical load as a rigid and elastic body. In the technique, the elasticity of the barrette body is considered by the finite element method, while that of the soil by flexibility coefficient method. The technique is applied efficiently for barrette group and barrette raft.

In this paper, the *CCT* is modified for analysing laterally loaded single barrettes. In which, the three-dimensional full interactions between the barrette and the surrounding soil are taken into consideration. Besides, *CCT* reduces considerably the number of equations to be solved, it enables applying the nonlinear response in lateral direction of the barrette by a hyperbolic relation between the load and displacement of the barrette.

## 2 Mathematical Modeling

The mathematical modelling of vertically loaded barrettes have been explained by El Gendy et al. (2016, 2017, 2018, 2019). The barrette is divided into a number of shaft and base elements with n nodes as

shown in Fig. 1, each one is acted upon by a distributed stress. To carry out the analysis, the stresses acting on the shaft and base elements are replaced by a series of concentrated forces acting on the nodes.

The displacement of the soil at any node $i$ of the barrette is written in general form as:

$$u_i = \sum_{j=1}^{n_s} Ix_{i,j}\, Qx_j \tag{1}$$

where $u_i$ soil displacement in x-direction on any shaft or base node $i$, m; $Qx_j$ contact force in x-direction on any shaft or base node $j$, kN; $n$ total number of nodes; and $Ix_{i,j}$ flexibility coefficient of node $i$ due to a concentrated force in x-direction on node $j$, m/kN.

Equations (1) for displacements of the soil adjacent to all nodes of the barrette is rewritten in a matrix form as:

$$\{u\} = [Ix]\{Qx\} \tag{2}$$

where $\{u\}$ $n$ displacement vector in x-direction; $\{Qx\}$ $n$ contact force vector in x-direction; and $[Ix]$ $n \times n$ soil flexibility matrix.

## 2.1 Flexibility Coefficients

Mindlin (1936) presented a mathematical solution for determining stresses and displacements in soil due to a point load acting beneath the surface of semi-infinite mass. The solution is often employed in the numerical analysis of piled foundations. Russo (2016) used this solution to predict the pile-soil interaction, based on a hybrid BEM approach.

According to *Mindlin's* solution, the displacement factor $fx_{ij}$ of point $i$ due to a point load $Qx_j$, kN, acting at point $j$ beneath the surface (Fig. 2) can be expressed as:

$$fx_{ij} = \frac{1}{16\pi G_s(1-\nu_s)} \left(\frac{3-4\nu_s}{R_1} + \frac{1}{R_2} + \frac{(x)^2}{R_1^3} + \frac{(3-4\nu_s)(x)^2 + 2cz}{R_2^3} - \frac{6cz(x)^2}{R_2^5} + \frac{4(1-\nu_s)(1-2\nu_s)}{R_2+z+c} - \frac{4(1-\nu_s)(1-2\nu_s)(x)^2}{R_2(R_2+z+c)^2}\right) \tag{3}$$

Where $R_1 = \sqrt{r^2+(z-c)^2}$, $R_2 = \sqrt{r^2+(z+c)^2}$; $c$ depth of the point load $Q_j$, kN from the surface, m; $z$ depth of the studied point $i$ from the surface, m; $r$ radial distance between points $i$ and $j$, m; $x$ horizontal distance in x-direction between points $i$ and $j$, m; $fx_{ij}$

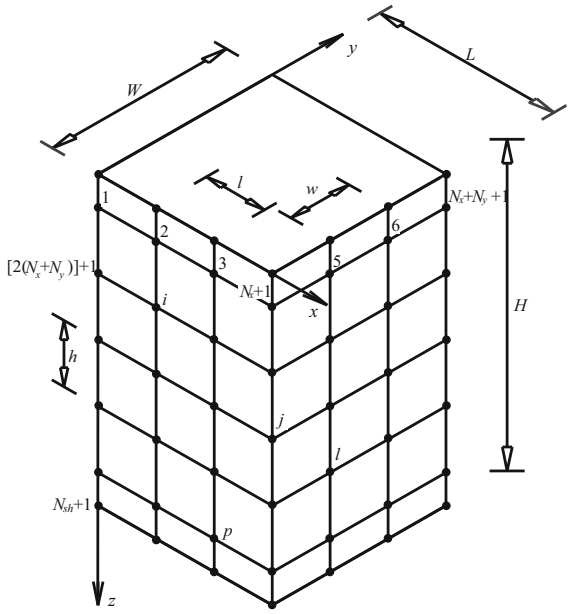


**Fig. 1** Single barrette geometry and elements

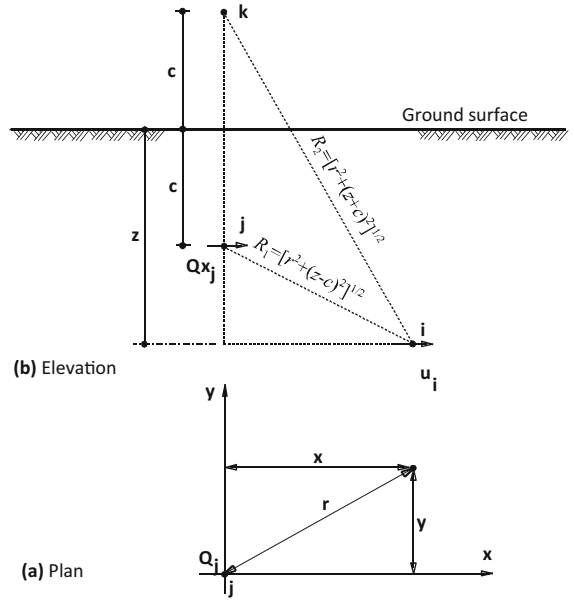


**Fig. 2** Geometry of point load beneath the surface

displacement factor of point $i$ due to a unit load in x-direction at point $j$, m/kN; $v_s$ *Poisson's* ratio of the soil.and $G_s$ shear modulus of the soil, kN/m$^2$.

$$G_s = \frac{E_s}{2(1+\nu_s)} \tag{4}$$

where $E_s$ Modulus of elasticity of the soil, kN/m$^2$.

Now, the displacement in x-direction $u_{ij}$, m, at point $i$ due to a point load $Qx_j$, kN, acting at point $j$ beneath the surface (Fig. 2) can be expressed as:

$$u_{ij} = Ix_{ij}\, Qx_j \tag{5}$$

or in matrix form:

$$\{u\} = [Ix]\{\, Qx\,\} \tag{6}$$

## 2.2 Soil Stiffness Matrix

To describe the formulation of composed coefficients for generating the soil stiffness matrix of the barrette in this case, consider, as an example, the simple barrette shown in Fig. 3a, which has a total of $n$ = 33 surface nodes in this case. The barrette of 3D is converted into a 1D model as presented in Fig. 3b, which has $n_b$= 4 nodes in 4 levels only. Each node has a force and a displacement in the horizontal direction. The unknowns of the problem will be reduced to $n_b$ contact forces $Qx_{bi}$ on soil-barrette interface and $n_b$ horizontal displacements $u_{bi}$ on all nodes of the barrette.

The soil stiffness matrix of Eq. (7) for the barrette shown in Fig. 3a can be expanded in the matrix form as:

$$\left\{\begin{Bmatrix} Qx_1 \\ \cdots \\ Qx_8 \end{Bmatrix}_1 \begin{Bmatrix} Qx_9 \\ \cdots \\ Qx_{16} \end{Bmatrix}_2 \begin{Bmatrix} Qx_{17} \\ \cdots \\ Qx_{24} \end{Bmatrix}_3 \begin{Bmatrix} Qx_{25} \\ \cdots \\ Qx_{33} \end{Bmatrix}_4\right\} = \begin{bmatrix} kx_{1,1} & \cdots & kx_{1,8} & kx_{1,9} & \cdots & kx_{1,16} & kx_{1,17} & \cdots & kx_{1,24} & kx_{1,25} & \cdots & kx_{1,33} \\ \cdots & \cdots & \cdots & \cdots & \cdots & \cdots & \cdots & \cdots & \cdots & \cdots & \cdots & \cdots \\ kx_{8,1} & \cdots & kx_{8,8} & kx_{8,9} & \cdots & kx_{8,16} & kx_{8,17} & \cdots & kx_{8,24} & kx_{8,25} & \cdots & kx_{8,33} \\ kx_{9,1} & \cdots & kx_{9,8} & kx_{9,9} & \cdots & kx_{9,16} & kx_{9,17} & \cdots & kx_{9,24} & kx_{9,25} & \cdots & kx_{9,33} \\ \cdots & \cdots & \cdots & \cdots & \cdots & \cdots & \cdots & \cdots & \cdots & \cdots & \cdots & \cdots \\ kx_{16,1} & \cdots & kx_{16,8} & kx_{16,9} & \cdots & kx_{16,16} & kx_{16,17} & \cdots & kx_{16,24} & kx_{16,25} & \cdots & kx_{16,33} \\ kx_{17,1} & \cdots & kx_{17,8} & kx_{17,9} & \cdots & kx_{17,16} & kx_{17,17} & \cdots & kx_{17,24} & kx_{17,25} & \cdots & kx_{17,33} \\ \cdots & \cdots & \cdots & \cdots & \cdots & \cdots & \cdots & \cdots & \cdots & \cdots & \cdots & \cdots \\ kx_{24,1} & \cdots & kx_{24,8} & kx_{24,9} & \cdots & kx_{24,16} & k_{24,17} & \cdots & kx_{24,24} & kx_{24,25} & \cdots & kx_{24,33} \\ kx_{25,1} & \cdots & kx_{25,8} & kx_{25,9} & \cdots & kx_{25,16} & kx_{25,17} & \cdots & kx_{25,24} & kx_{25,25} & \cdots & kx_{25,33} \\ \cdots & \cdots & \cdots & \cdots & \cdots & \cdots & \cdots & \cdots & \cdots & \cdots & \cdots & \cdots \\ kx_{33,1} & \cdots & kx_{33,8} & kx_{33,9} & \cdots & kx_{33,16} & kx_{33,17} & \cdots & kx_{33,24} & kx_{33,25} & \cdots & kx_{33,33} \end{bmatrix} \left\{\begin{Bmatrix} u_1 \\ \cdots \\ u_8 \end{Bmatrix}_1 \begin{Bmatrix} u_9 \\ \cdots \\ u_{16} \end{Bmatrix}_2 \begin{Bmatrix} u_{17} \\ \cdots \\ u_{24} \end{Bmatrix}_3 \begin{Bmatrix} u_{25} \\ \cdots \\ u_{33} \end{Bmatrix}_4\right\} \tag{8}$$

Inverting the soil flexibility matrix in Eqs. (6) leads to:

$$\{\, Qx\,\} = [\,kx\,]\{u\} \tag{7}$$

where $[kx]$ are $n \times n$ soil stiffness matrix, $[kx] = [Ix]^{-1}$.

where $kx_{i,\,j}$ is stiffness coefficient of the soil stiffness matrix, kN/m.

To reduce the size of the problem, the barrette is represented by a vertical line member having a variable horizontal displacement along its height. Then, the displacement in every barrette level node in 1D is considered to be constant. Another point of view in choosing this idea is that the designer is interested in the soil displacement and contact forces at different levels on the barrette height not at each barrette node.

This assumption can establish the relationship between the displacement and force on each node in 1D. It can be done by equating all displacements in each barrette level in 3D by a uniform displacement. In Eq. (8), the summation of rows and columns corresponds to the barrette node $i$ in 1D, leads to:

$$\begin{Bmatrix} \left\{\sum_{i=1}^{8} Qx_i\right\}_1 \\ \left\{\sum_{i=9}^{16} Qx_i\right\}_2 \\ \left\{\sum_{i=17}^{24} Qx_i\right\}_3 \\ \left\{\sum_{i=25}^{33} Qx_i\right\}_4 \end{Bmatrix} = \begin{bmatrix} \sum_{i=1}^{8}\sum_{j=1}^{8} kx_{i,j} & \sum_{i=1}^{8}\sum_{j=9}^{16} kx_{i,j} & \sum_{i=1}^{8}\sum_{j=17}^{24} kx_{i,j} & \sum_{i=1}^{8}\sum_{j=25}^{32} kx_{i,j} \\ \sum_{i=9}^{16}\sum_{j=1}^{8} kx_{i,j} & \sum_{i=9}^{16}\sum_{j=9}^{16} kx_{i,j} & \sum_{i=9}^{16}\sum_{j=17}^{24} kx_{i,j} & \sum_{i=9}^{16}\sum_{j=25}^{32} kx_{i,j} \\ \sum_{i=17}^{24}\sum_{j=1}^{8} kx_{i,j} & \sum_{i=17}^{24}\sum_{j=9}^{16} kx_{i,j} & \sum_{i=17}^{24}\sum_{j=17}^{24} kx_{i,j} & \sum_{i=17}^{24}\sum_{j=25}^{32} kx_{i,j} \\ \sum_{i=25}^{33}\sum_{j=1}^{8} kx_{i,j} & \sum_{i=25}^{33}\sum_{j=9}^{16} kx_{i,j} & \sum_{i=25}^{33}\sum_{j=17}^{24} kx_{i,j} & \sum_{i=25}^{33}\sum_{j=25}^{33} kx_{i,j} \end{bmatrix} \begin{Bmatrix} \left\{\sum_{i=1}^{8} u_i\right\}_1 \\ \left\{\sum_{i=9}^{16} u_i\right\}_2 \\ \left\{\sum_{i=17}^{24} u_i\right\}_3 \\ \left\{\sum_{i=25}^{33} u_i\right\}_4 \end{Bmatrix} \tag{9}$$

where $Kx_{i,j}$ composed coefficient, kN/m; $u_{bi}$ displacement in x-direction in node $i$ of 1D barrette, m; $u_{b1} = u_{1=} \; u_{2=} \ldots = u_8$, $u_{b2} = u_9 = \ldots = u_{16,\ldots\ldots}$, $u_{b4} = u_{25} = \ldots = u_{33}$; $Qx_{bi}$ contact force on node $i$ of 1D barrette, kN; $Qx_{b1=} \; Qx_{1+} \; Qx_{2+\ldots} + Qx_8$, $Qx_{b2=} \; Qx_{9} + \ldots + Qx_{16,\ldots\ldots}$, $Qx_{b4=} \; Qx_{25+\ldots} + Qx_{33}$;

Accordingly, Eq. (9) of the soil stiffness matrix can be rewritten for the barrette of 1D in composed coefficients as:

$$\begin{Bmatrix} Qx_{b1} \\ Qx_{b2} \\ Qx_{b3} \\ Qx_{b4} \end{Bmatrix} = \begin{bmatrix} Kx_{b1,1} & Kx_{b1,2} & Kx_{b1,3} & Kx_{b1,4} \\ Kx_{b2,1} & Kx_{b2,2} & Kx_{b2,3} & Kx_{b2,4} \\ Kx_{b3,1} & Kx_{b3,2} & Kx_{b3,3} & Kx_{b2,4} \\ Kx_{b4,1} & Kx_{b4,2} & Kx_{b4,3} & Kx_{b2,4} \end{bmatrix} \begin{Bmatrix} u_{b_1} \\ u_{b_2} \\ u_{b_3} \\ u_{b_4} \end{Bmatrix} \tag{10}$$

Equation (10) shows that the soil stiffness matrix in Eq. (8) of size 33 × 33 is reduced considerably to an equivalent soil stiffness matrix of size 4 × 4. It could be written in a compacted form as presented in Eq. (7).

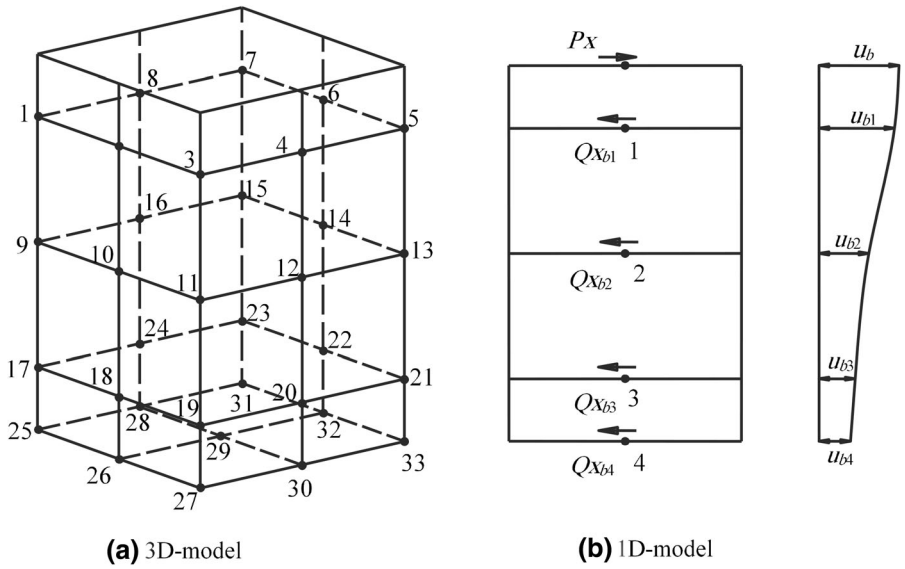


**(a)** 3D-model **(b)** 1D-model

**Fig. 3** Surface mesh of the barrette with node numbering, lateral loads and displacement

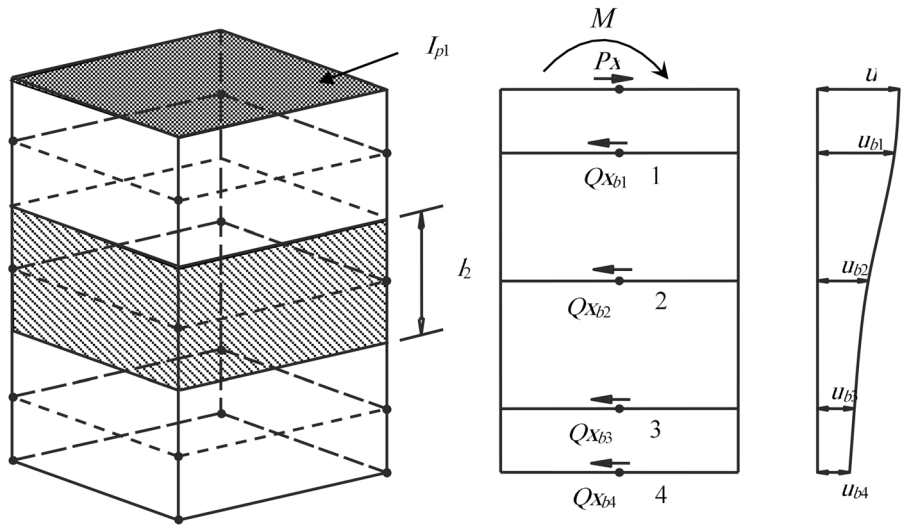


**(a)** Barrette model in 1D-FE **(b)** Forces and displacement in barrette

**Fig. 4** Finite element mesh of barrette and element geometry

## 2.3 Barrette Stiffness Matrix

The finite element method is used for analysing the barrette body, which is exposed to external forces on the soil-barrette interface as soil reactions in addition to the applied load on its head as an action. The compatibility between the horizontal displacements of the barrette and the soil displacements at the soil-barrette interface is taken in the horizontal direction. The composed coefficient technique is used to formulate the soil stiffness matrix for the barrette as a line member from the original soil stiffness matrix of Eq. (8). This soil stiffness matrix takes also into account the interaction effect among all the soil-barrette interface nodes.

From the finite element, the beam stiffness matrix of the barrette element $i$ can be expressed as (Fig. 4):

$$[kx]_i = \frac{Ep \cdot Ip_i}{L_i^3} \begin{bmatrix} 12 & 6L & -12 & 6L \\ 6L & 4L^2 & -6L & 2L^2 \\ 12 & 6L & -12 & 6L \\ 6L & 2L^2 & -6L & 4L^2 \end{bmatrix} \tag{11}$$

where $Ep$ Modulus of Elasticity of the barrette material, kN/m$^2$; $Ip_i$ moment of inertia of the barrette element $i$, m$^4$; and $L_i$ length of the barrette element $i$, m.

According to the finite element method, the assembled stiffness matrix equation for the barrette is:

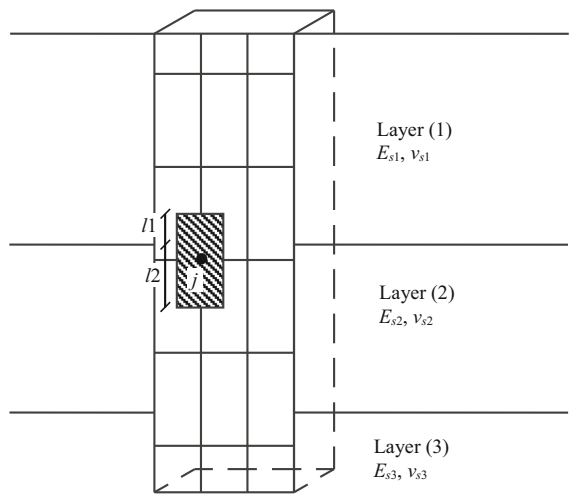


**Fig. 5** Geometry of shaft element lies between two layers

$$[kx]\{\delta x\} = \{Px\} - \{Qx_b\} \tag{12}$$

where $\{\delta x\}$ $n_b$ deformation vector; $\{u_1, \theta_1, u_2, \theta_2, u_3, \theta_3, u_4, \theta_4\}$; $\{Px\}$ $n_b$ vector of applied load on the barrette, $\{Px_1, Mx_1, 0, 0, \ldots, 0\}$; and $[kx]$ $(2 \times n_b)$-$\times$ $(2 \times n_b)$ beam stiffness matrix.

Substituting Eqs. (7) into (12), leads to:

$$[kx]\{\delta x\} = \{Px\} - [kx_b]\{u_b\} \tag{13}$$

Assuming full compatibility between barrette displacement $u_i$ and soil displacement $u_{bi}$, the following equation can be obtained:

$$[[kx] + [kx_b]]\{\delta x\} = \{Px\} \tag{14}$$

Solving the above system of linear equations, gives the displacement and rotation at each node, which is equal to the soil deformation at that node. Substituting soil displacement from Eqs. (14) into (12), gives contact forces $Qx_{bi}$ on the barrette.

### 2.4 Multi-layered Soil

In case of vertical loads *Mindlin's* solution is applied for isotropic elastic half-space soil medium. For finite layer, flexibility coefficients for vertical load may be obtained as described by Poulos and Davis (1968). As an example, for a point $k$ in a layer of depth $h$, the flexibility coefficient is then:

$$f_{k,j}(h) = f_{k,j}(\infty) - f_{h,j}(\infty) \tag{15}$$

where $f_{k,\,j}(h)$ flexibility coefficient for a point $k$ in a layer of depth $h$ due to a unit vertical load on point $j$, m/kN; $f_{k,\,j}(\infty)$ flexibility coefficient for a point $k$ due to a unit vertical load on point $j$ in a semi-infinite mass, m/kN; $f_{h,\,j}(\infty)$ flexibility coefficient for a point within the semi-infinite mass directly beneath $k$, at a depth $h$ below the surface due to a unit vertical load on point $j$, m/kN.

For horizontal loads, when computing displacement $u_{i,j}$, the *Mindlin's* solution is applied by characterizing the soil layers around the barrette by *Young's* Modulus and *Poisson's* ratio of points $j$, where $u_{i,j}$ is lateral soil displacement on any shaft or base node $i$ due to a lateral point load at point $j$.

If the shaft element cross two soil layers as shown in Fig. 5, the soil properties will take as a ratio of the length of the cross element to each layer.

$$E_s = \frac{E_{s1}\, l_1 + E_{s2}\, l_2}{l_1 + l_2} \tag{16}$$

$$v_s = \frac{v_{s1}\, l_1 + v_{s2}\, l_2}{l_1 + l_2} \tag{17}$$

where $E_s$ and $v_s$ are soil properties, which applied in the *Mindlin's* solution.

### 2.5 Nonlinear Analysis of Barrette

Russo (1998) presented a numerical method for the analysis of piled raft where piles were modelled as interactive linear or non-linear springs. The nonlinear relation between the load and settlement of a barrette may be determined by considering a hyperbolic relation between load on the barrette head *Ph* and the settlement *wn* as shown in Fig. 6 and Eq. 18. *Russo* et al. (2012) and *Russo* (2018) applied efficiently the hyperbolic relation to re-assessment of foundation settlements for the Burj Khalifa, the tallest building all over the world.

Russo (2016) developed a computer code, based on a hybrid BEM approach, to predict the pile-soil interaction. The code is used to throw light on the mechanism of the pile-soil interaction under horizontal loading. He considered the nonlinear response of pile load settlement in horizontal direction through the hyperbolic relation.

The nonlinear behavior of the barrette load-settlement in vertical direction is:

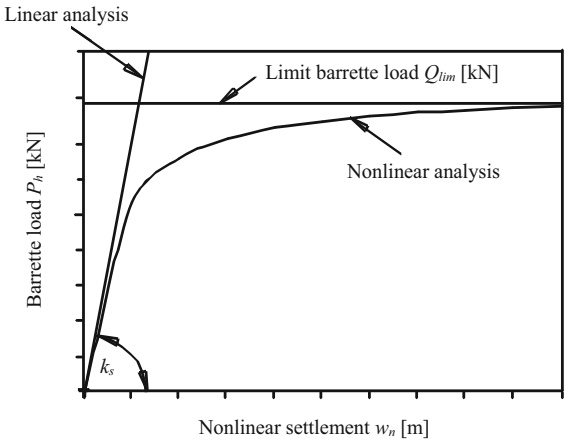


**Fig. 6** Load-settlement curve of a barrette (hyperbolic relation)

**Table 1** Loads and barrette geometries

| Case | Load (kN) | Height (m) | Cross section |
|---|---|---|---|
| 1 | 3000 | 15 | 0.5 m × 0.5 m |
| 2 | 2500 | 10 | 0.7 m × 0.7 m |
| 3 | 10,000 | 40 | 2.8 m × 0.8 m |
| 4 | 8000 | 30 | 2.7 m × 1.2 m |

**Table 2** Barrette material properties

| |
|---|
| Modulus of Elasticity of the barrette material $E_c = 2.5 \times 10^7$ kN/m$^2$ |
| Poisson's ratio of the barrette material $\nu_c = 0.20$- |

**Table 3** Subsoil properties

| Case | Layer No. | Soil type | $z$ m | $E_s$ kN/m$^2$ | $\nu_s$ |
|---|---|---|---|---|---|
| 1 | 1 | Stiff clay | 2 | 10,000 | 0.40 |
| | 2 | Loose sand | 5 | 15,000 | 0.35 |
| | 3 | Silt | 10 | 30,000 | 0.30 |
| | 4 | Dense sand | $\infty$ | 100,000 | 0.15 |
| 2 | 1 | Stiff clay | 1 | 10,000 | 0.40 |
| | 2 | Loose sand | 5 | 15,000 | 0.35 |
| | 3 | Silt | 8 | 30,000 | 0.30 |
| | 4 | Dense sand | $\infty$ | 80,000 | 0.20 |
| 3 | 1 | Very stiff clay | 5 | 20,000 | 0.35 |
| | 2 | Loose sand | 15 | 25,000 | 0.30 |
| | 3 | Silt | 35 | 30,000 | 0.30 |
| | 4 | Dense sand | $\infty$ | 80,000 | 0.20 |
| 4 | 1 | Very stiff clay | 2 | 15,000 | 0.40 |
| | 2 | Loose sand | 12 | 25,000 | 0.30 |
| | 3 | Silt | 22 | 30,000 | 0.30 |
| | 4 | Dense sand | $\infty$ | 100,000 | 0.15 |

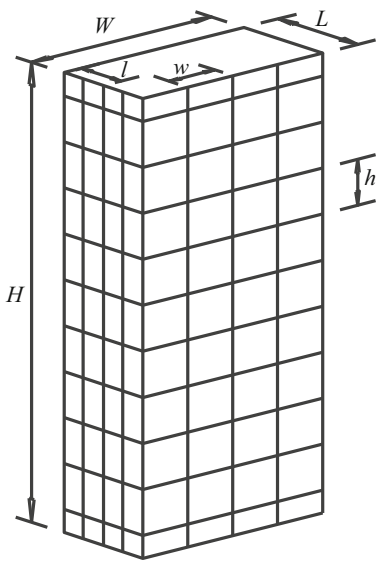


**Fig. 7** Surface element of the barrette for the four cases

$$P_h = \frac{w_n}{\frac{1}{k_s} + \frac{w_n}{Q_{\text{lim}}}} \tag{18}$$

while in horizontal direction is:

$$P_x = \frac{u_n}{\frac{1}{k_x} + \frac{u_n}{H_{\text{lim}}}} \tag{19}$$

where $w_n$ is nonlinear settlement of the barrette, m; $Q_{l\text{im}}$ is vertical limit load, kN; $u_n$ is nonlinear displacement in x-direction of the barrette, m; $H_{l\text{im}}$ is horizontal limit load, kN.

In Fig. 6, the initial tangent modulus for barrette is easily obtained from linear analysis of the barrette, which is equal to the modulus of soil stiffness $k_s$. the vertical limit load $Q_{lim}$ is a geometrical parameter of the hyperbolic relation. This can be applied also for horizontal direction.

## 3 Numerical Results

The developed program *ELPLA* is used to analyse single barrettes with both linear and nonlinear subsoil models under vertical and lateral loads using flexibility coefficient and composed coefficient technique (*CCT*). To verify the validity of this program and its mathematical methods and subsoil models, some

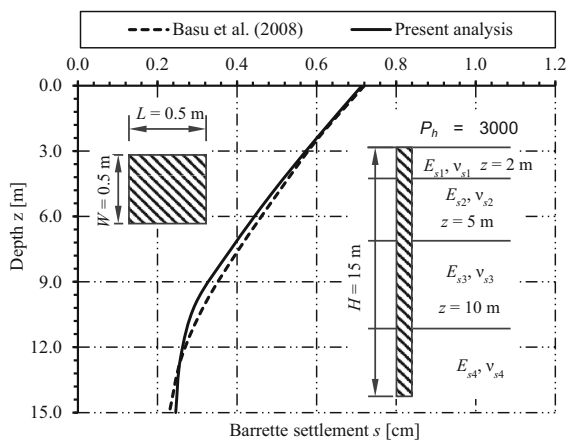


**Fig. 8** Settlement along the barrette height (case 1)

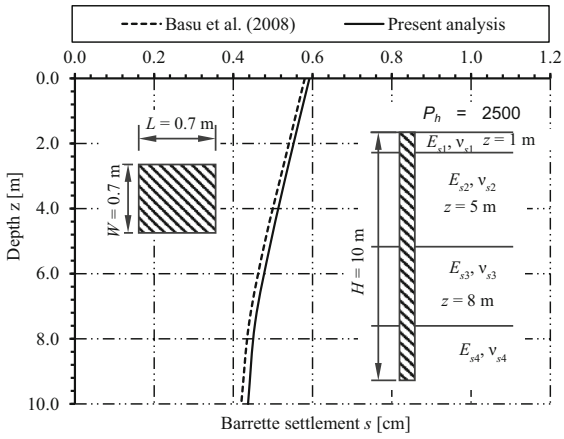


**Fig. 9** Settlement along the barrette height (case 2)

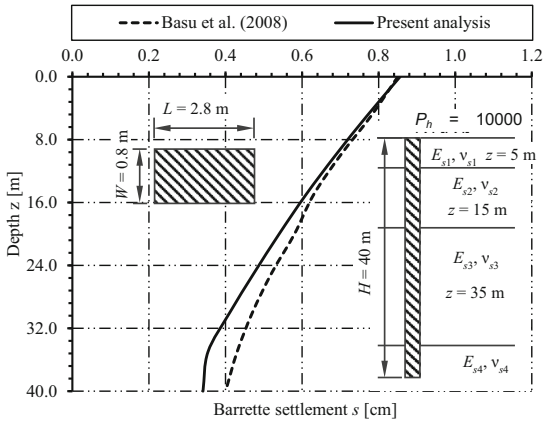


**Fig. 10** Settlement along the barrette height (case 3)

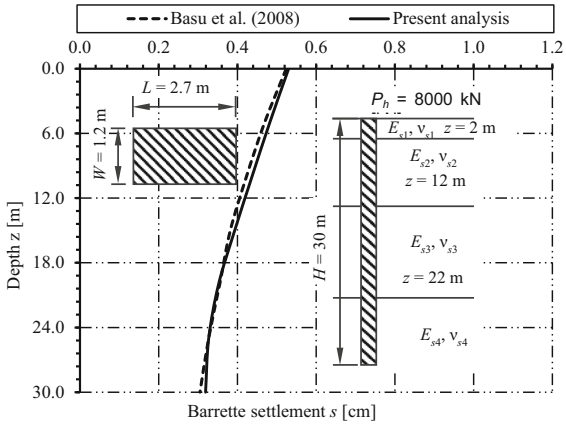


**Fig. 11** Settlement along the barrette height (case 4)

problems published previously by researchers using different methods of analysis and models are compared with the results obtained by the analysis used in this paper.

### 3.1 Validity of Linear Analysis of Vertically Loaded Single Barrette

An analytical analysis of a single barrette having a rectangular cross section embedded in a multi-layered soil medium is available in the reference Basu et al. (2008). In the analytical analysis, the differential equations governing the displacements of the barrette-soil system were obtained using the variation principles. Closed-form solutions for barrette deflection and axial force along the barrette shaft were then produced by using the method of initial parameters.

The barrette is considered and analysed for four different cases under different loads, geometries and subsoil conditions. The load on the barrette head and barrette geometry for the chosen cases are listed in Table 1. The barrette material properties are listed in Table 2. The subsoil of each case consists of four layers, each layer has a different Modulus of Elasticity, $E_s$ and *Poisson's* ratio, $\nu_s$ are listed in Table 3.

A comparison of results of the single barrette in a multi-layered soil medium of the present analysis with those by Basu et al. (2008) is presented herein. The height of the barrette is divided into equal elements of $h = 1$ m each in all cases. Both the barrette length and

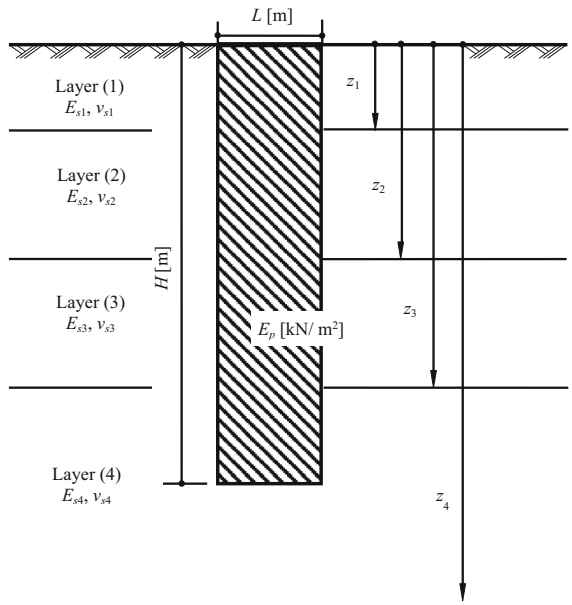


**Fig. 12** Subsoil of single barrette

width are divided into four equal elements in each case, as shown in Fig. 7. In the analysis, barrette material is considered to be elastic and the barrette is analysed as 1D finite elements.

The barrette settlement, *s* along the barrette height obtained from the present analysis for the four cases of analysis are compared with those by Basu et al. (2008) in Figs. 8, 9, 10 and 11.

From these results, it can be concluded that the absolute difference between the computed barrette head settlements in the present analysis and those by Basu et al. (2008) is 0.01 cm for all cases. In addition, the absolute differences between the computed barrette base settlements is 0.02 cm for the first case, 0.01 cm for the second and fourth cases, and 0.06 cm for case (3).

These results show also that results of the present analysis are in a good agreement with the analytical results obtained by Basu et al. (2008). Results of the barrette head settlements are similar to those by *Basu* et al. (2008). However, regarding results of the base settlements, the difference reached 15.0% in case of a barrette having a great aspect ratio in the cross section, case (3). The difference in this case is very small when compared to the barrette dimensions, which equals to 0.06 cm.

### 3.2 Validity of Linear Analysis of Laterally Loaded Single Barrette

To verify the present analysis of a laterally loaded single barrette in multi-layered soil, the barrette displacements with barrette heights obtained by the present analysis of a laterally loaded single barrette using flexibility coefficient and *CCT* are compared with those obtained by Basu and Salgado (2007, 2008) and Choi et al. (2014, 2015).

An analytical analysis of a laterally loaded single barrette embedded in a multi-layered soil medium is available in the references Basu and Salgado (2007, 2008) and Choi et al. (2014, 2015) and compared with those by equivalent 3D-FE using ABAQUS. In the analytical analysis, the differential equations governing the displacements of the barrette-soil system were obtained using variational principles. Closed-form solutions for barrette displacement and forces along the barrette shaft were then produced by using the method of initial parameters for analysis a circular pile with an equivalent diameter with the same second moment of inertia as that of the barrette.

The single barrette shown in Fig. 12 is analysed for seven different cases with different geometries, lateral loads, and subsoil conditions. Barrettes geometry, lateral loads on the barrettes head and modulus of elasticity of barrettes $E_p$ for the chosen cases are listed in Table 4. The subsoil of each case consists of different layers, each layer has a different modulus of elasticity $E_s$ and *Poisson's* ratio $\nu_s$ are listed in Table 5.

A comparison of results of the laterally loaded single barrette in a multi-layered soil medium of the present analysis with those by Basu and Salgado (2007, 2008) and Choi et al. (2014, 2015) is presented here. Both the barrette length and width are taken as two elements and the height of the barrette is divided into equal elements with $h = 0.5$ m, in all cases as shown in Fig. 13 except case (3) the barrette length and width are taken as four elements and the height of the barrette is divided into equal elements with $h = 2$ m as shown in Fig. 7. In the analysis, the barrette material is considered to be elastic and the barrette is analysed as 1D finite elements as shown in Fig. 14.

The barrette displacement $u$ and bending moment along the barrette height obtained from the present

**Table 4** Barrette geometries, loads and material

| Case | Cross section | Height (m) | $E_p$ (kN/m$^2$) | Load (kN) |
|---|---|---|---|---|
| 1 | 0.50 m × 0.50 m | 10 | $24 \times 10^6$ | 300 |
| 2 | 0.70 m × 0.40 m | 15 | $24 \times 10^6$ | 300 |
| 3 | 2.80 m × 0.80 m | 40 | $25 \times 10^6$ | 3000 |
| 4 | 0.70 m × 0.40 m | 10 | $25 \times 10^6$ | 300 |
| 5 | 0.53 m × 0.53 m | 10 | $25 \times 10^6$ | 300 |
| 6 | 0.70 m × 0.40 m | 15 | $24 \times 10^6$ | 300 |
| 7 | 0.50 m × 0.50 m | 15 | $25 \times 10^6$ | 500 |

**Table 5** Soil properties

| Case | Layer No. | Soil type | z (m) | $E_s$ (kN/m$^2$) | $\nu_s$ |
|---|---|---|---|---|---|
| 1, 2, 4, 5 | 1 | Very stiff clay | 2 | 20,000 | 0.35 |
| | 2 | Medium sand | 5 | 35,000 | 0.25 |
| | 3 | Dense sand | 8 | 50,000 | 0.20 |
| | 4 | Dense sand | ∞ | 80,000 | 0.15 |
| 3 | 1 | Very stiff clay | 1.5 | 20,000 | 0.35 |
| | 2 | Loose sand | 3.5 | 25,000 | 0.30 |
| | 3 | Medium sand | 8.5 | 40,000 | 0.25 |
| | 4 | Dense sand | ∞ | 80,000 | 0.20 |
| 6 | 1 | Dense sand | ∞ | 50,000 | 0.20 |
| 7 | 1 | Medium sand | ∞ | 40,000 | 0.25 |

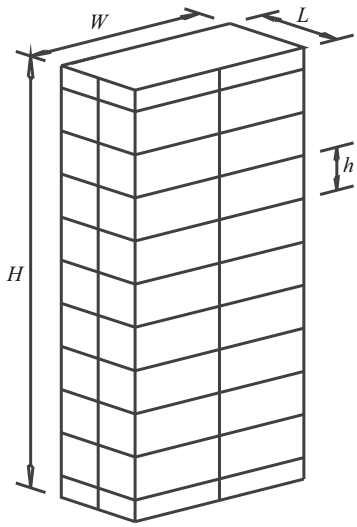


**Fig. 13** Surface element of the barrette for all cases except case (3)

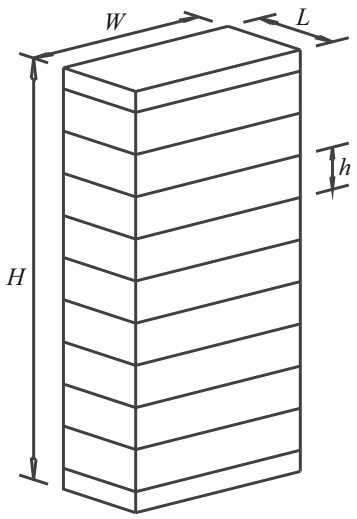


**Fig. 14** Barrette representing by 1D finite elements

analysis using flexibility coefficient and *CCT* for the seven cases of analysis are compared with those by Basu and Salgado (2007, 2008) and Choi et al. (2014, 2015) as shown in Figs. 15, 16, 17, 18, 19, 20, 21, 22 and 23.

Results show that the absolute difference between the barrette head displacements in the present analysis and that by Basu and Salgado (2007, 2008) and Choi et al. (2014, 2015) is less than 0.05 cm for all cases except case (3) which is 0.11 cm. This difference when using FEA is less than 0.08 cm for cases (1), (2) and (6) and 0.2 cm for case (3).

In addition, the absolute difference between the computed barrette base displacements in the present

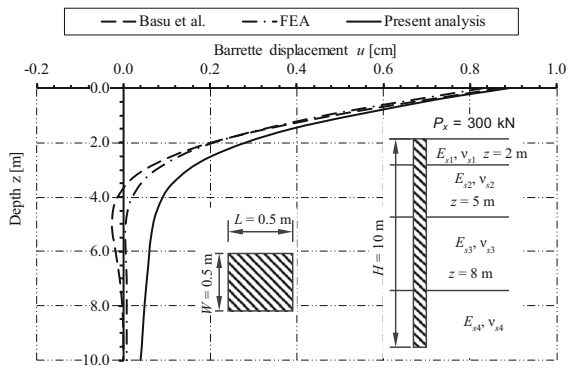


**Fig. 15** Displacement $u$ cm with the barrette height (case 1)

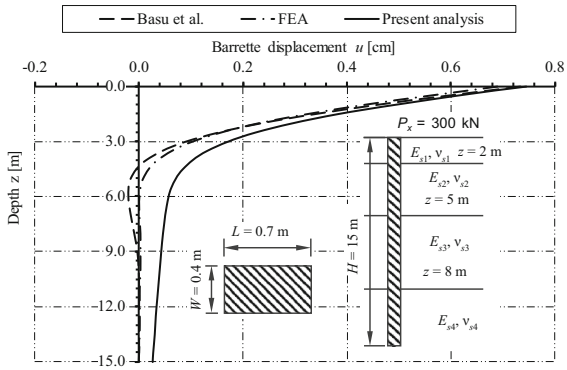


**Fig. 16** Displacement *u* cm with the barrette height (case 2)

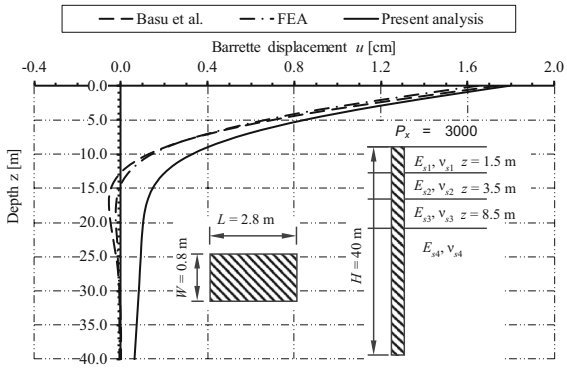


**Fig. 17** Displacement *u* cm with the barrette height (case 3)

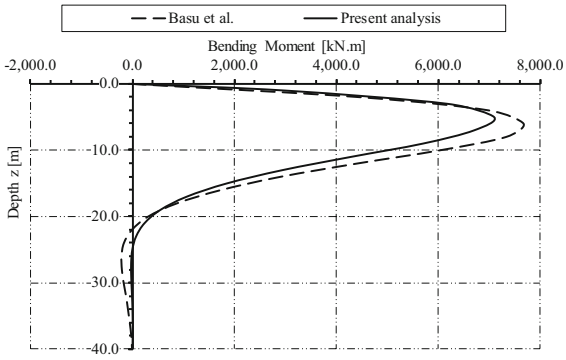


**Fig. 18** Bending moment kN.m with the barrette height (case 3)

analysis and those by Basu and Salgado (2007, 2008) and Choi et al. (2014, 2015) is less than 0.04 cm for all cases except case (3) which is 0.06 cm. This difference when using FEA is less than 0.03 cm for cases (1), (2) and (6) and 0.07 cm for case (3).

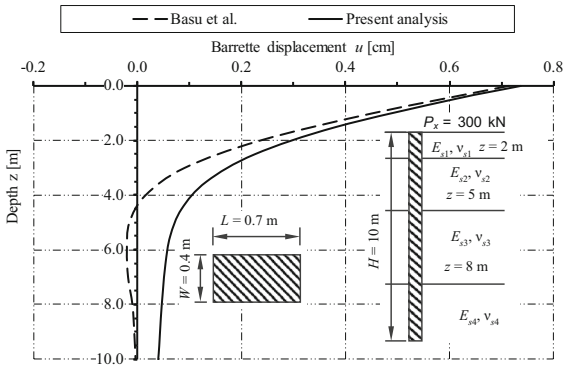


**Fig. 19** Displacement *u* cm with the barrette height (case 4)

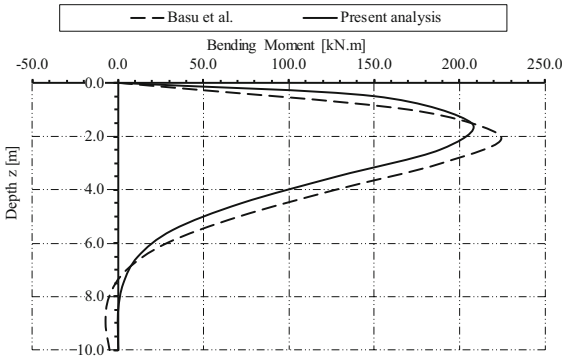


**Fig. 20** Bending moment kN.m with the barrette height (case 4)

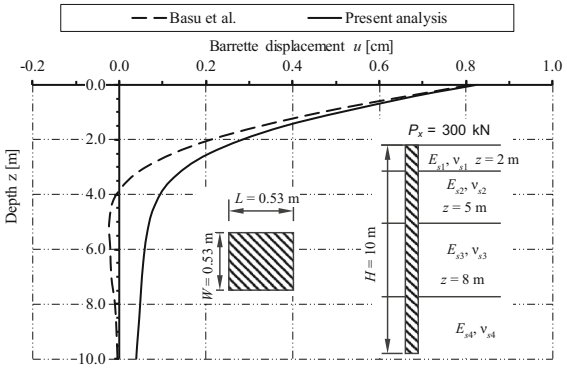


**Fig. 21** Displacement *u* cm with the barrette height (case 5)

Comparing the maximum bending moment using the present analysis and those from Basu and Salgado (2007, 2008) and Choi et al. (2014, 2015), the differences is less than 11%.

In general, it can be concluded that results of the present analyses using flexibility coefficient and *CCT*

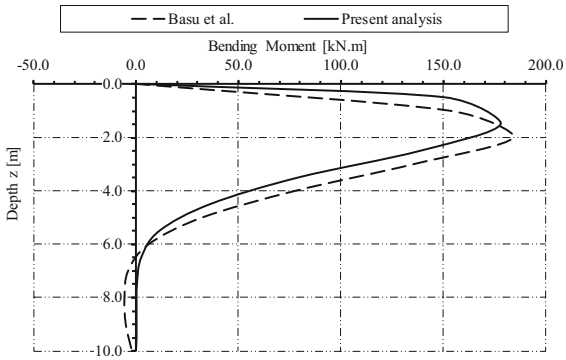


**Fig. 22** Bending moment kN.m with the barrette height (case 5)

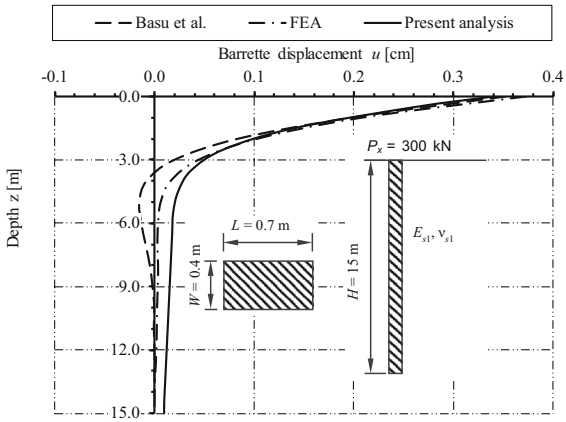


**Fig. 23** Displacement *u* cm with the barrette height (case 6)

are in a good agreement with both analytical results and numerical results using full 3D FEA.

### 3.3 Validity of Nonlinear Analysis of Single Barrette

To verify the present nonlinear analysis of a vertically and laterally loaded single barrette, the barrette results obtained by the present nonlinear analysis are compared with those obtained by Poulos and Small (2019) using 3D FE and using an equivalent circular shafted pile to represent the barrette.

The barrette geometry, material and soil properties are shown in Fig. 24. The subsoil is consisting of two layers, each layer having a different Modulus of Elasticity $E_s$ and *Poisson's* ratio $v_s$.

A comparison between results of the present analysis with those by Poulos and Small (2019) are

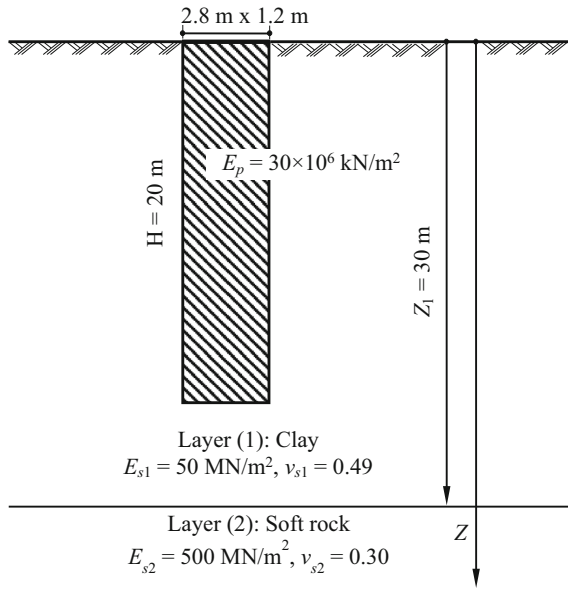


**Fig. 24** Single barrette with subsoil

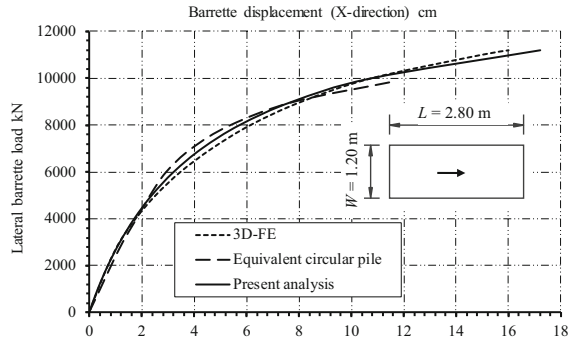


**Fig. 25** Load displacement curve of barrette 20 m height (X-direction)

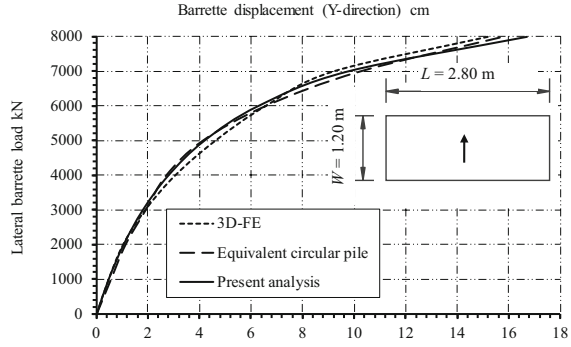


**Fig. 26** Load displacement curve of barrette 20 m height (Y-direction)

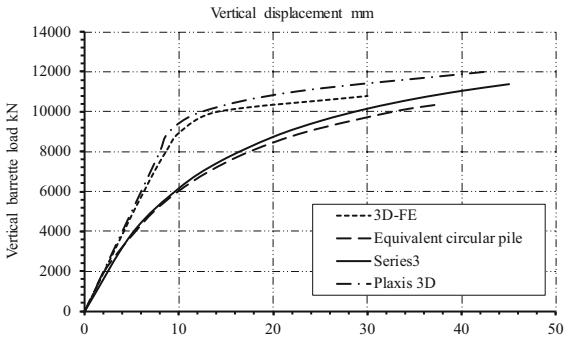


**Fig. 27** Vertical load displacement curve of barrette 20 m height

presented herein. The height of the barrette is divided into equal elements, each element has a height of $h$ = 1.0 m. Both the barrette length and width are taken as two elements, as shown in Fig. 13. In the analysis, barrette material is considered elastic and the barrette is analysed as 1D Finite Element. The barrettes are analysed nonlinearly using a hyperbolic function to represent the real load–displacement relation. Limit vertical loads was $Q_{lim}$ = 15 MN, while for lateral loads were $H_{lim}$ = 14.5 MN for load in x-direction and $H_{lim}$ = 10 MN for load in y-direction. These limit loads are assumed from the load–displacements curves presented by Poulos and Small (2019) .

The lateral load–displacement curves of the barrette 20 m height in both X and Y-directions obtained from the present analysis are compared in Figs. 25 and 26 with those obtained by Poulos and Small (2019) . Figure 27 shows the vertical load–displacement curves for the barrettes obtained from the present

**Table 6** Barrette geometries and material

| Cross section | Height (m) | $E_p$ (kN/m$^2$) | References |
|---|---|---|---|
| 3.0 m × 1.5 m | 57.5 | 37 × 10$^6$ | Rafa and Moussai (2018) |
| 2.82 m × 0.64 m | 52.5 | 37 × 10$^6$ | Znamenskii et al. (2019) |

**Table 7** Subsoil properties, Bangkok, Rafa and Moussai (2018)

| Layer No. | Soil type | $z$ (m) | $E_s$ (MN/m$^2$) | $\nu_s$ | $C$ (kN/m$^2$) | ° | $_{sat}$ (kN/m$^3$) | $_{unsat}$ (kN/m$^3$) |
|---|---|---|---|---|---|---|---|---|
| 1 | Soft clays | 13.5 | 5 | 0.3 | 10 | 23 | 16.5 | 16 |
| 2 | Stiff clays | 26.0 | 60 | 0.3 | 25 | 26 | 18 | 17 |
| 3 | Dense sands | 36.0 | 90 | 0.3 | – | 36 | 19.5 | 18.5 |
| 4 | Hard clays | 54.0 | 100 | 0.3 | 40 | 24 | 20 | 19 |
| 5 | Dense sands | 100.0 | 100 | 0.3 | – | 36 | 20 | 19 |

**Table 8** Subsoil properties, Moscow, Znamenskii et al. (2019)

| Layer No. | Soil type | $z$ (m) | $E_s$ (MN/m$^2$) | $\nu_s$ | $C$ (kN/m$^2$) | (°) | (kN/m$^3$) |
|---|---|---|---|---|---|---|---|
| 1 | Fine sands | 4.0 | 7 | 0.3 | 13 | 17 | 18.1 |
| 2 | Very soft loam | 8.5 | 21 | 0.3 | 2 | 27 | 19.2 |
| 3 | Sands | 16.5 | 30 | 0.3 | 1 | 29 | 19.9 |
| 4 | Half hard clays | 20.5 | 56 | 0.3 | 79 | 16 | 18.1 |
| 5 | Hard clays | 24.5 | 51 | 0.3 | 93 | 21 | 18.6 |
| 6 | Hard clays | 47.5 | 56 | 0.3 | 66 | 21 | 21.7 |
| 7 | Limestone | 70.0 | 6800 | 0.25 | $Rc$ = 34 MPa | | 18.5 |

Where $Rc$ is ultimate strength in uniaxial compression

analysis with that obtained by Poulos and Small (2019).

These results show that the present nonlinear analyses are in a good agreement with those by Poulos and Small (2019).

In case of laterally loaded barrette, the load–displacement curve depends on the direction of loading. As reported before by Zhang (2003), El Wakil and Nazir (2013) and Poulos and Small (2019), when the barrette is loaded along the major axis, it is predicted to carry more load and have a stiffer response than when loaded along the minor axis. This is due to the high resistance of the barrette loaded along the minor axis.

In case of axially loaded barrette, Poulos and Small (2019) use a value of $R_f = 0.8$ in the Equivalent circular pile model to make the curve flatter, were $R_f$ is the ratio between limit load and ultimate load. As reported before by Poulos and Small (2019), the effect of having no interface elements make the curve steeper when using 3D-FE.

### 3.4 Comparative Examination Between the Present Analysis and Vertical Load Tests

Load tests of single barrettes having a rectangular cross section embedded in a multi-layered soil medium are available in the references of Rafa and Moussai (2018) and Znamenskii et al. (2019). In these load tests, results of barrette load tests are obtained from Bangkok, Thailand subsoil area and Moscow, Russia subsoil area respectively.

Barrettes geometry and modulus of elasticity of barrettes $E_p$ for the chosen cases are listed in Table 6.

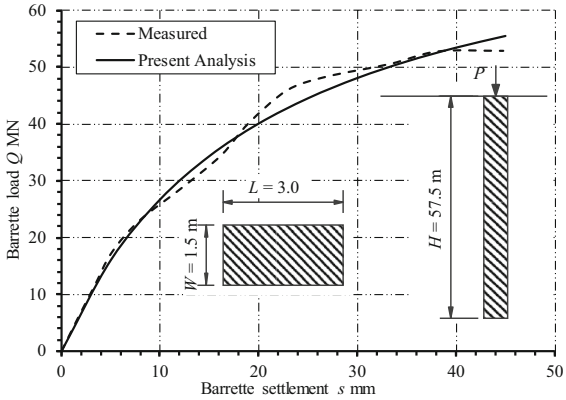


**Fig. 28** Load settlement curve, Rafa and Moussai (2018)

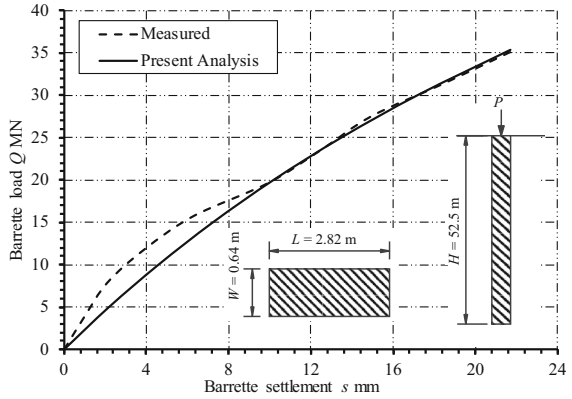


**Fig. 29** Load settlement curve, Znamenskii et al. (2019)

**Table 9** Barrette geometries

| Case | Cross section | Height (m) | $E_p$ (kN/m$^2$) |
|---|---|---|---|
| 1 | 2.80 m × 0.80 m | 51 | 30.3 × 10$^6$ |
| 2 | 2.70 m × 1.20 m | 30 | 35 × 10$^6$ |

The subsoil of each case consists of different layers, each layer has different properties as listed in Tables 7 and 8.

Comparisons of the results of single barrettes in a multi-layered soil medium of the present analysis with those obtained by Rafa and Moussai (2018) and Znamenskii et al. (2019) are presented herein, the height of the barrettes is divided into equal elements, each element has a height of $h = 2$ m. Both the barrettes length and width are divided into four equal elements, as shown in Fig. 7. Barrettes are analysed nonlinearly using a hyperbolic function to represent the real load-settlement relation. In the analysis, in case of comparing with Rafa and Moussai (2018) the barrette is assumed to be fully rigid having a uniform settlement, while in case of comparing with Znamenskii et al. (2019) the barrette is analysed as elastic body due to the very high strength of the limestone layer.

The limit barrette loads $Q_{lim}$ are considered to be 80 and 110 MN, which are assumed from the load settlement curves of Rafa and Moussai (2018) and Znamenskii et al. (2019) respectively.

The barrette load-settlement relations obtained from the present nonlinear analysis are compared with those by the load tests carried out by Rafa and

**Table 10** Soil properties

| case | Layer No. | Soil type | $z$ (m) | Ava. *SPT* | $E_s$ (kN/m$^2$) | $\nu_s$ |
|---|---|---|---|---|---|---|
| 1 | 1 | Fill (Clayey silty sand with gravel and occasional cobble/boulder) | 1.5 | 19 | 13,600 | 0.3 |
| | 2 | | 8 | 53 | 27,200 | 0.3 |
| | 3 | | 11 | 10 | 10,000 | 0.3 |
| | 4 | Fill (Cobbles) | 15 | 29 | 17,600 | 0.3 |
| | 5 | Alluvium (Clayey silty sand with gravel) | 23 | 13 | 11,000 | 0.3 |
| | 6 | Completely decomposed granite (Silty sand with gravel) | 29.5 | 40 | 22,000 | 0.3 |
| | 7 | | 32.5 | 77 | 36,600 | 0.3 |
| | 8 | | 34 | 104 | 47,600 | 0.3 |
| | 9 | | 40 | 144 | 63,900 | 0.3 |
| | 10 | | 100 | 194 | 83,600 | 0.3 |
| 2 | 1 | Fill (Clayey silty sand with gravel and occasional cobble/boulder) | 15 | 27 | 33,200 | 0.3 |
| | 2 | Marine deposit (Clayey silty sand) | 19.5 | 18 | 24,000 | 0.3 |
| | 3 | Alluvium (Clayey silty sand with gravel) | 28 | 35 | 40,750 | 0.3 |
| | 4 | Completely decomposed granite (Silty sand with gravel) | 29.5 | 63 | 69,000 | 0.3 |
| | 5 | | 34 | 46 | 52,000 | 0.3 |
| | 6 | | 100 | 68 | 74,000 | 0.3 |

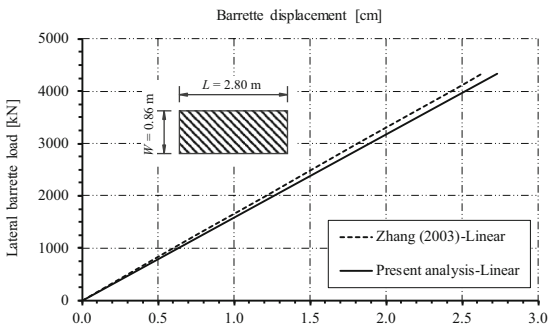


**Fig. 30** Linear load displacement curve of the barrette, case (1)

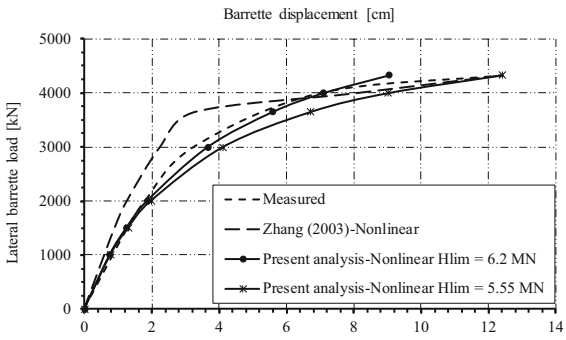


**Fig. 31** Nonlinear load displacement curve of the barrette, case (1)

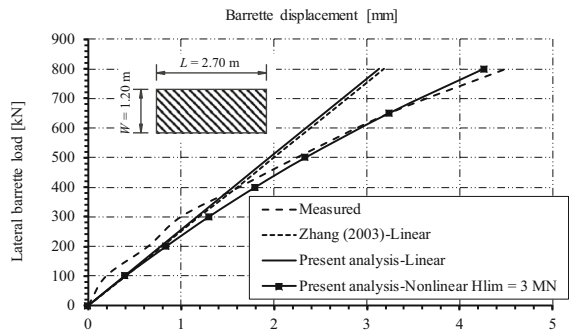


**Fig. 32** Load displacement curve of the barrette, case (2)

Moussai (2018) and Znamenskii et al. (2019) in Figs. 28 and 29, respectively. From these figures, it can be concluded that the difference in settlements values were 0.4 cm and 0.14 cm compared with those by Rafa and Moussai (2018) and Znamenskii et al. (2019), respectively. They are very small when compared to the barrette dimensions.

The verification shows that the load-settlement behaviour of the present nonlinear analyses are in a good agreement with the measured load-settlements carried out by Rafa and Moussai (2018) and Znamenskii et al. (2019).

### 3.5 Comparative Examination Between the Present Analysis and Lateral Load Tests

Lateral load–displacement relation of the barrette obtained by the present analysis is compared with that obtained by Zhang (2003) from load tests of a laterally loaded single barrette and from numerical analysis using 3D FE.

Load tests of single barrettes having a rectangular cross section embedded in a multi-layered soil medium are available in the reference Zhang (2003). In the load tests, results of barrette load tests are obtained from Hong Kong subsoil areas.

The barrette is considered and analysed for different cases. The barrette geometry and modulus of elasticity $E_p$ for the chosen cases are listed in Table 9. The soil properties, modulus of elasticity $E_s$ and *Poisson's* ratio $\nu_s$ are listed in Table 10. $E_s$ was estimated from SPT according to Bowles (1996).

The height of the barrette is divided into equal elements, each element has a height of $h$ = 2.0 m for case (1) and 1.0 m for case (2). Both the barrette length and width are taken as two elements as shown in Fig. 13. The barrettes are analysed nonlinearly using a hyperbolic function. Horizontal limit loads have been assumed from load displacement curves of Zhang (2003). These were 6 MN and 5.45 MN for the first case and 3 MN for the second case.

The horizontal load–displacement relation of the barrette obtained from the present analysis is compared in Figs. 30, 31 and 32 with that obtained from load tests and from 3D FE carried out by Zhang (2003).

From comparison of the linear analysis, it found that the absolute difference between displacements presented by Zhang (2003) and those of the present analysis is less than 0.1 cm in case (1) and 0.05 mm in case (2).

For nonlinear analysis, the difference between the displacement of the present analysis for $H_{lim}$ = 6 MN and the measured displacement is less than 0.31 cm in case (1), except when the load is 4330 kN, the difference is 3.21 cm. However, for $H_{lim}$ = 5.45 MN, the absolute difference is increased to 1.90 cm, when the load is 4000 kN. Then, the difference decreased to 0.05 cm, when the load is 4330 kN. In case (2), the difference is less than 0.43 mm. These differences are very small when compared to the barrette dimensions.

Finally, the verification shows that the lateral load–displacement behaviour of the present linear and nonlinear analyses are in a good agreement with those of the measured load tests and 3D FE carried out by Zhang (2003).

## 4 Conclusions

An application on laterally loaded single barrettes using the composed coefficient technique and flexibility matrix is presented. The proposed technique considers the three dimensional full interactions between the single barrette and the soil. From application of *CCT* technique, it can be concluded that:

- The technique can be effectively used in linear and nonlinear analyses of vertically and laterally loaded single barrette in layered soil medium.
- Due to the lower number of nodes in the converted one dimensional model rather than three dimensional finite element model, the first model consumes less computation time in the analysis. This enables the technique to be used for analysing large barrette foundations such as barrette group and barrette raft.
- As in the technique, the barrette elements are composed in one member, the analysis can be used easily for predicting the nonlinear response of the lateral load-displacement of the barrette using a hyperbolic relation between the lateral load and displacement under both axial and lateral loads.
- Verification examination of the present analysis for analysing vertically and laterally loaded barrettes show that results are in a good agreement with those obtained numerically by 3D FE.
- Good agreement is noticed between results of the nonlinear analysis for analysing both vertically and horizontally loaded barrette and measured values obtained from barrette load tests.
- Although the barrette head displacements of the present linear analysis for laterally loaded barrettes are very close when compared with those obtained numerically by 3D FE, the distribution of barrette lateral displacements along the barrette length is relatively softer (giving higher displacements) in the present analysis. However, the absolute difference in results of the base displacements is very

small, which is less than 0.1 cm, when compared to the barrette dimensions. In which, the barrette head displacement is the effective displacement is this case of analysis.

## References


ABAQUS 6.13 [Computer software]. Providence, RI, Dassault Systèmes

Abdel Glil E, El Gendy M, Ibrahim H, Reda A (2009) Optimization of piled raft in port-said. Port-Said Eng Res J 13(1):27–45

Basu D, Salgado R (2007) Elastic analysis of laterally loaded pile in multi-layered soil. Geomech Geoengin 2(3):183–196. https://doi.org/10.1080/17486020701401007

Basu D, Salgado R (2008) Analysis of laterally loaded piles with rectangular cross sections embedded in layered soil. Int J Numer Anal Meth Geomech 32(7):721–744. https://doi.org/10.1002/nag.639

Basu D, Prezzi M, Salgado R, Chakraborty T (2008) Settlement analysis of piles with rectangular cross sections in multi-layered soils. Comput Geotech 35(4):563–575. https://doi.org/10.1016/j.compgeo.2007.09.001

Bowles J (1996) Foundation analysis and design, 5th edn. McGraw-Hill, New York

Choi Y, Basu D, Salgado R, Prezzi M (2014) Response of laterally loaded rectangular and circular piles in soils with properties varying with depth. J Geotech Geoenviron Eng. https://doi.org/10.1061/(ASCE)GT.1943-5606.0001067

Choi Y, Basu D, Prezzi M, Salgado R (2015) Study on laterally loaded piles with rectangular and circular cross sections. Geomech Geoeng 10(2):139–152. https://doi.org/10.1080/17486025.2014.902119

Conte E, Troncone A, Vena A (2013) Nonlinear three-dimensional analysis of reinforced concrete piles subjected to horizontal loading. Comput Geotech 49:123–133. https://doi.org/10.1016/j.compgeo.2012.10.013

El Gendy M (2007) Formulation of a composed coefficient technique for analyzing large piled raft. Ain Shams Eng J 42:29–56

El Gendy M, El Gendy A (2019) Analysis and design of raft and piled Raft-Program ELPLA. GEOTEC Software Inc., Calgary

El Gendy M, El Araby I, El Labban A (2010a) Comparative studies for piled raft resting on port said clay. Port-Said Eng Res J 14(2):1–15

El Gendy M, El Azab M, Mobarak W (2010b) Effect of tie girders on piled footing in port-said. Port-Said Eng Res J 14(1):27–45

El Gendy M, El Araby I, Kamal M (2013) Comparative Examination of Single Bored Piles Using International Codes. Scientific Research Journal of Engineering 5(10):796–806. https://doi.org/10.4236/eng.2013.510096

El Gendy M, El Araby I, Kamal M (2014) Comparative analysis of large diameter bored piles using international codes. Deep Found Inst J 8(1):15–26. https://doi.org/10.1179/1937525514Y.0000000001

El Gendy M, Ibrahim H, El Araby I (2016) Analyzing barrettes as large-section supports by CCT. Port-Said Eng Res J 20(2):27–39. https://doi.org/10.21608/pserj.2016.33578

El Gendy M, Ibrahim H, El Araby I (2017) Analyzing single barrette as rigid support by composed coefficient technique. Malays J Civil Eng 29(3):273–288. https://doi.org/10.11113/mjce.v29.53

El Gendy M, Ibrahim H, El Araby I (2018) Modeling Single barrettes as elastic support by CCT. Malays J Civil Eng 30(2):296–312. https://doi.org/10.11113/mjce.v30n2.481

El Gendy M, Ibrahim H, El Araby I (2019) Composed coefficient technique for modelling barrette groups. Malays J Civil Eng 31(1):23–33. https://doi.org/10.11113/mjce.v31n1.510

El Kamash W, El Gendy M, Salib R, Kandil M (2014) Studying of shear walls with piled raft over soft soil against seismic loads. Port-Said Eng Res J 18(1):144–152. https://doi.org/10.21608/pserj.2014.46816

El Wakil AZ, Nazir A (2013) Behavior of laterally loaded small scale barrettes in sand. Ain Shams Eng J 4(3):343–350. https://doi.org/10.1016/j.asej.2012.10.011

Ibrahim F, El Gendy M, Salib R, El Kamash W (2009) Nonlinear analysis of piled raft with 3D-space structure. Port-Said Engi Res J 13(2):27–45

Lei G, Hong X, Shi J (2007) Approximate three-dimensional analysis of rectangular barrette-soil-cap interaction. Can Geotech J 44(7):781–796. https://doi.org/10.1139/t07-017

Lin S, Lu F, Kuo C, Su T, Mulowayi E (2014) Axial capacity of barrette piles embedded in gravel layer. J Geoeng 9:103–107. https://doi.org/10.6310/jog.2014.9(3).3

MIDAS GTS NX [Computer software], MIDAS Information Technology Co., KOREA.

Mindlin D (1936) Force at a point in the interior of a semi-infinite solid. Physics 7(5):195–202. https://doi.org/10.1063/1.1745385

Mohamedien M, El Gendy M, El Araby I, El Azab M, Moubarak A (2013) Reducing settlement using piled raft for neighboring foundations in port-said. Port-Said Eng Res J 17(2):136–146. https://doi.org/10.21608/pserj.2013.50588

PLAXIS 3D [Computer software], Delft, Netherlands

Poulos H, Davis E (1968) The settlement behaviour of single axially loaded incompressible piles and piers. Géotechnique 18(3):351–371. https://doi.org/10.1680/geot.1968.18.3.351

Poulos HG, Small JC (2019) The use of equivalent circular piles to model the behaviour of rectangular barrette foundations. Geotech Eng J SEAGS AGSSEA 50(3):106–109

Rabiei M (2015) Piled raft design strategies for high rise buildings. Geotech Geol Eng 34(1):75–85. https://doi.org/10.1007/s10706-015-9929-x

Rabiei M, Choobbasti A (2018) Economic design optimization of piled raft foundations. Innov Infrastruct Solut 3(1):75–85. https://doi.org/10.1007/s41062-018-0170-3

Rabiei M, Choobbasti A (2019) Innovative piled raft foundations design using artificial neural network. Front Struct Civil Eng. https://doi.org/10.1007/s11709-019-0585-8

Rafa S, Moussai B (2018) Three-dimensional analyses of bored pile and barrette load tests subjected to vertical loadings.

Soil Mech Found Eng 55(3):146–152. https://doi.org/10.1007/s11204-018-9518-0

Russo G (1998) Numerical analysis of piled rafts. Int J Numer Anal Meth Geomech 22(6):477–493. https://doi.org/10.1002/(SICI)1096-9853(199806)22:6%3C477:AID-NAG931%3E3.0.CO;2-H

Russo G (2016) A method to compute the non-linear behaviour of piles under horizontal loading. Soils Found 56(1):33–43. https://doi.org/10.1016/j.sandf.2016.01.003

Russo G (2018) Analysis and design of pile foundations under vertical load: an overview. Rivista Italiana di Geotecnica 52(2):52–71. https://doi.org/10.19199/2018.2.0557-1405.52

Russo G, Abagnara V, Poulos HG, Small J (2012) Re-assessment of foundation settlements for the Burj Khalifa. Dubai. Acta Geotechnica 8(1):3–15. https://doi.org/10.1007/s11440-012-0193-4

Seo H, Basu D, Prezzi M, Salgado R (2009) Load-settlement response of rectangular and circular piles in multilayered soil. J Geotech Geoenviron Eng 135(3):420–430. https://doi.org/10.1061/(ASCE)1090-0241(2009)135:3(420)

Thasnanipan N, Maung A, Tanseng P (1998) Barrettes Founded in Bangkok Subsoils Construction and Performance. The Thirteenth Southeast Asian Geotechnical Conference, Taipei, Taiwanpp, pp. 573-578

Zhang L (2003) Behavior of laterally loaded large-section barrettes. J Geotech Geoenviron Eng 129(7):639–648. https://doi.org/10.1061/(ASCE)1090-0241(2003)129:7(639)

Znamenskii V, Bakholdin V, Parfenov A, Musatova M (2019) Investigation of the load-carrying capacity of barretes for a 56-storey residential building. Soil Mech Found Eng 56(1):1–6. https://doi.org/10.1007/s11204-019-09561-2